Highly Efficient Ultra-Broadband Terahertz Modulation Using Bi-Directional Switching of Liquid Crystals

*Xuequan Chen, Kaidi Li, Rui Zhang, Swadesh Kumar Gupta, Abhishek Kumar Srivastava and Emma Pickwell-MacPherson**

Dr. Xuequan Chen, Mr. Kaidi Li, Prof. Emma Pickwell-MacPherson
Department of Electronic Engineering, The Chinese University of Hong Kong, Hong Kong, 999077, China

Dr. Rui Zhang
Shenzhen Institutes of Advanced Technology, Chines Academy of Science, Shenzhen, 518055, China

Dr. Swadesh Kumar Gupta, Prof. Abhishek Kumar Srivastava
Department of Electronic and Computer Engineering, The Hong Kong University of Science and Technology, Hong Kong, 999077, China

Prof. Emma Pickwell-MacPherson
Physics Department, Warwick University, Coventry CV4 7AL, UK.
E-mail: E.pickwell.97@cantab.net

Keywords: terahertz modulation, quarter wave, liquid crystal, polarization switch, broadband

Accurately manipulating field strength and polarization state are essential in various terahertz applications. Such manipulations are based on the efficient modulation of the amplitude and phase of electromagnetic waves. However, there is a lack of such terahertz modulators with sufficient efficiency and bandwidth. In this article, the Brewster-critical angle is exploited for modulation by using a nematic liquid crystal. Unlike liquid crystal phase shifters that only give a narrow-band phase delay via a one-directional switch, the presented device modulates both the amplitude and phase across an ultrabroad bandwidth via a bi-directional active switch. An average intensity modulation depth over 99.6% is achieved for 0.2-1.6 THz. Furthermore, highly accurate polarization conversion between linear and circular states is also realized for 0.4-1.8 THz, with the average degree of linear and circular polarizations as high as 0.994 and 0.998 respectively. The superior accuracy, bandwidth and active control achieved provide great potential for multifunctional terahertz modulation.

1. Introduction

Electromagnetic waves can be described by electric-field (E-field) vectors expressed in a complex form of amplitude and phase. Efficiently modulating these two physical properties allows precise control of the polarization state and light intensity, which is essential for a wide range of applications. For example, in the terahertz (THz) range, field strength needs to be well controlled in nonlinear optics[1,2], field-effects on gene expressions[3] and compressed sensing imaging[4]. Polarization manipulation is crucial for chiral spectroscopy[5,6], anisotropy ellipsometry[7,8] and communications[9]. The growth of THz spectrometers promotes these applications and the requirement on adaptive broadband and accurate modulators[10,11]. Controlling field strength is relatively easy and has been realized based on a variety of mechanisms. Metamaterials are frequently used to enhance the light-material interaction to give a deep and fast modulation, with various semiconducting[12,13] and two-dimensional materials[14–17]. However, their common shortfall is the narrow working bandwidth. Phase-transition materials such as vanadium dioxide have also been adopted[18,19]. Their huge conductivity change enables a good modulation depth, but their high temperature sensitivity makes them difficult to be stably modulated[20]. Moving one step forward to modulate amplitude and phase simultaneously is more challenging. The Goos–Hänchen shift can be utilized for achieving frequency-dependent dispersion[21]. Metamaterials are still a popular candidate for narrow-band polarization switching[22,23]. Stacked metallic gratings were implemented to relatively extend the working bandwidth[24–27], which is still limited due to the Fabry-Perot effect.

Utilizing the birefringence of nematic liquid crystals (LCs) for phase shifting is a common technique at optical frequencies, and it has also been studied in the THz range. The biggest challenge for LC THz devices comes from the need to increase the LC cell depth to be wavelength-comparable to provide an adequate phase delay. For example, the typical E7 LC with a refractive index birefringence of 0.15 needs a 500 μm thickness to produce a 90^0

phase delay above 1 THz[28], hence results in a very long recovery time over a few minutes. Thicker LC cells may produce up to 2π phase delay, but with an even slower speed[29]. Strong magnetic fields may accelerate the speed but controlling in this way is typically bulky and inflexible[30,31]. Searching for LCs with a larger birefringence or separating the LC cell into multiple layers are the two major approaches to address the phase retardance and speed requirements[32–34]. However, the improvement is very limited. The largest birefringence reported in the THz range is 0.33[32], and the maximum number of LC layers reported is two[34,35] (due to the larger insertion loss and more challenging fabrications). The work by B. Vasić solved this problem by employing a metal-insulator-metal structure to realize a quarter-wave conversion with a LC layer of only few micrometers[36]. However, the narrow operation frequency is decided by the structural dimensions and it is not tunable. Another two challenges of THz LC devices are the lack of transparent electrodes and the narrow working bandwidth. The plasma frequencies of most conductive materials are above the THz range. The widely used optically transparent materials such as ITO[35], ITO nanowires[28] or graphene[37] show considerable absorptions and reflections at THz frequencies. Metallic gratings give a high transparency but are polarization-selective to support only a linear output[38,39]. The narrow working bandwidth is a basic property for LC shifters due to the wavelength-dependent phase delay. Although the operation frequency can be tuned by the voltage, the much slower tuning speed compared to optical LC devices makes it impractical for THz spectroscopy. The above difficulties strongly limit the application of LC devices in the THz range.

In this work, we propose a silicon (Si) sandwich structure Si-LC-Si coupled with a 30^0 Si prism for amplitude and phase modulation. The Si works as a dense medium (with a much larger refractive index compared to the RDP 94990 LC) to provide a sensitive Brewster-critical angle change by tuning the orientations of the LC molecules, which releases a great

modulation potential. More importantly, the Si enables the device to be actively controlled in two directions. Its semiconducting nature make it a perfectly transparent electrode for transferring the bias voltage on the LC, whilst its high resistivity also makes it a resistor to allow an E-field to be generated across the wafer to significantly improve the recovery speed. We theoretically and experimentally demonstrate that at the incident angle of 27.7^0 , it can deeply modulate the broadband THz with very low loss. Furthermore, at the incident angle of 30^0 , active switch between linear-circular polarization can be achieved in an ultra-broad band range with superior accuracy.

2. Theory and experimental results

2.1. Optical modeling

Si has a refractive index of 3.42 for 0.2 - 4 THz[40], which is much larger than that of most LCs (typically from 1.5 to 1.8). The great sensitivity of the p-reflection coefficients on the incident angles can be deduced from the equation for Brewster angle $\theta_B = \mathrm{atan}(n_2/n_1)$ and the equation for critical angle $\theta_c = \mathrm{asin}(n_2/n_1)$, where n_2 and n_1 are the refractive indexes of the refracted and incident medium respectively. *atan* and *asin* functions give similar values when the input is close to zero. Therefore, when n_1 is sufficiently larger than n_2 to give a small ratio, the resulting Brewster angle will be very close to the critical angel. This indicates that a sharp change in the reflectivity from zero to one, as well as a rapid phase change of 180^0 can be achieved by tuning the incident angle over only a small range. Although altering the incident angle is impractical in a measurement, varying the refractive index n_2 is possible by employing LCs. Thus by careful control of the refractive index, the Brewster and critical angles (i.e. the reflection dependence on the incident angle) can be manipulated to provide a dramatic change in the reflection for a specific incident angle. To our best knowledge, this is

the first time the sensitive Brewster-critical reflection change by LC control is proposed and applied for efficient amplitude and phase modulation in the THz range.

The actual reflection from the Si-LC interface is an isotropic-uniaxial reflection determined by the optical axis orientation of the LC molecules. The reflection coefficients can be calculated from the Maxwell boundary conditions and have been theoretically derived by J. Lekner[41,42]. From his theory, the reflection can be analytically calculated by specifying the optical axis orientation of the LC. Here, we use this theory to calculate the Si-LC reflection for different LC orientations.

2.2. Device configuration and characterization

As shown in Figure 1a, the device consists of a Si/LC/Si structure coupled with a 30^0 Si prism. The whole device was placed on top of a copper heat sink with liquid cooling. The incident plane lies in the x-z plane and the reflected THz beam was modulated by the device. The 3D cross-section view of the Si-LC-Si structure is illustrated in Figure 1b. Both Si wafers are 2-inch p-type Si with a resistivity of 3000 Ω·cm. Each Si wafer has two parallel aluminium electrodes fabricated by photolithography. The electrode edges are along the x-direction and a 1.5 cm Si gap is left in-between the electrodes. The current-voltage curves of both Si wafers were characterized and the linear relationship indicates an ideal ohmic contact (see Supporting Information Section 1). SD1 alignment layers were spin coated on both wafers with a thickness around 10 nm to initially align the LC in the y-direction. A 500 μm dielectric spacer was inserted in-between the wafers and left a 2×2 cm^2 area for accommodating the liquid crystal. Before assembling the wafers and the spacer, a near-infrared microscope covering the 1 - 2 μm transparent wavelength of Si was used to precisely align the electrodes on the two wafers, with a misalignment error less than 20 μm in the y-direction. Details of the near-infrared alignment are shown in Supporting Information Section

2. Finally, the RDP 94990 LC (DIC, Japan) was filled in and the device was sealed. The left electrodes of the upper wafer and the right electrode of the lower wafer were permanently connected to 0V (GND) and a positive voltage (+U) respectively, while the left electrode of the lower wafer and the right electrode of the upper wafer were connected to GND and +U through a switch.

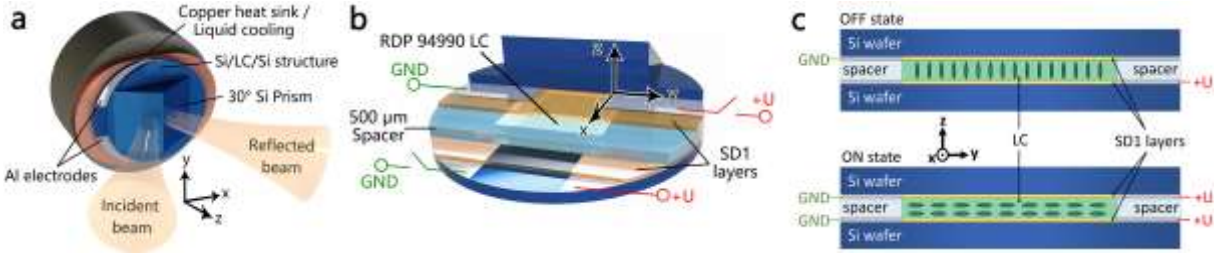

Figure 1. Optical arrangement and device configuration. **a.** Device assembled on a liquid-cooling cooper heat sink and illuminated by the THz light. **b.** 3D cross-section view of the y-z and x-y planes. **c.** 2D cross section view of the y-z plane in the OFF and ON states.

Figure 1c shows the y-z cross section view of the device in the OFF (up) and ON (low) states. When the switch was OFF, a +U voltage was loaded on the LC in z-direction because the resistivity of the LC was orders of magnitude higher than that of the Si. The OFF state rotated the LC molecules into the z-direction. When the switch was ON, the +U voltage was loaded across both Si wafers in the same y-direction. The ohmic contacts ensure the voltage is fully loaded on the wafers, and the previous infrared alignment of the upper and lower electrodes ensures the E-field being generated in the z-direction due to the misalignment is less than 4% of the y-directional field. The combined E-field will be in the y-direction with an orientation error smaller than 2.3^0 . Therefore, the ON state gives a y-directional rotational force, which is the same as the SD1 alignment direction, to actively improve the recovery speed. It is worth mentioning here that the approach in our THz in plane and THz out of plane (Tip-Top) LC device (which was able to be actively switched in two directions)[39] was not applicable here because the grating design only allows a linear polarization output. Furthermore, the in-plane switch could not fully rotate the LC molecules into the vertical direction, resulting in a phase delay of only 35^0 at 2 THz. Similar limitations also occur in the work by Vieweg et al[43].

Here, for the first time, our new Si-electrode design enables full electrical control in two exactly perpendicular directions without any limitation on the output polarization.

The RDP 94990 LC was first characterized by measuring the Si/LC/Si structure in transmission by a free-space THz time-domain spectroscopy (TDS) system at 18^0 C. The refractive index and absorption coefficient of the ordinary and extraordinary directions are shown in Figure 2. The result matches well with our previous characterization[44]. The refractive indices in the ordinary and extraordinary directions have very small dispersions from 0.1 THz to 3 THz. The absorption coefficients in both directions are very close and remain low over the full spectrum.

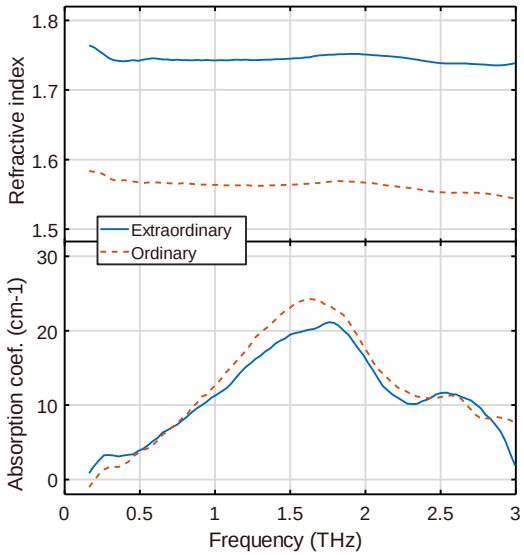

Figure 2. Characterized refractive index and absorption coefficient of the RDP 94990 LC in ordinary and extraordinary directions.

2.3. Intensity modulation

The p-reflection from the Si-LC interface when the optical axis of the LC was aligned in the y- and z-directions were calculated according to J. Lekner's theory[42] and shown in Figure 3a. The complex refractive indices of the LC used in the calculation are n_o=1.57-0.025i and n_e=1.74-0.025i (the averaged value across 0.1 - 2 THz). This gives a good estimation for this frequency range due to the very small dispersion. As expected from the analysis, Figure 3a

shows that the difference between the Brewster angle and the critical angle for both curves is as close as 4^0 . The two curves are off-set by about 3^0 , thus the change in the reflection under a specific incident angle is dramatic. The most obvious point will be at an incident angle of 27.7^0 as it reaches the Brewster angle when the LC molecules were aligned in the z-direction and gives rise to a near-zero reflection. Tuning the LC molecules into the y-direction changes the angle to be near critical and returns a near total-internal reflection. The reflection amplitude changing from 0.03 to 0.76 indicates a very deep intensity modulation of 99.9%, which is calculated by $100\% \times \left(1 - \left|r_{min}^2\right|/\left|r_{max}^2\right|\right)$. The insertion loss from the LC reflection is also as low as 2 dB ($20 \times \lg 0.76$).

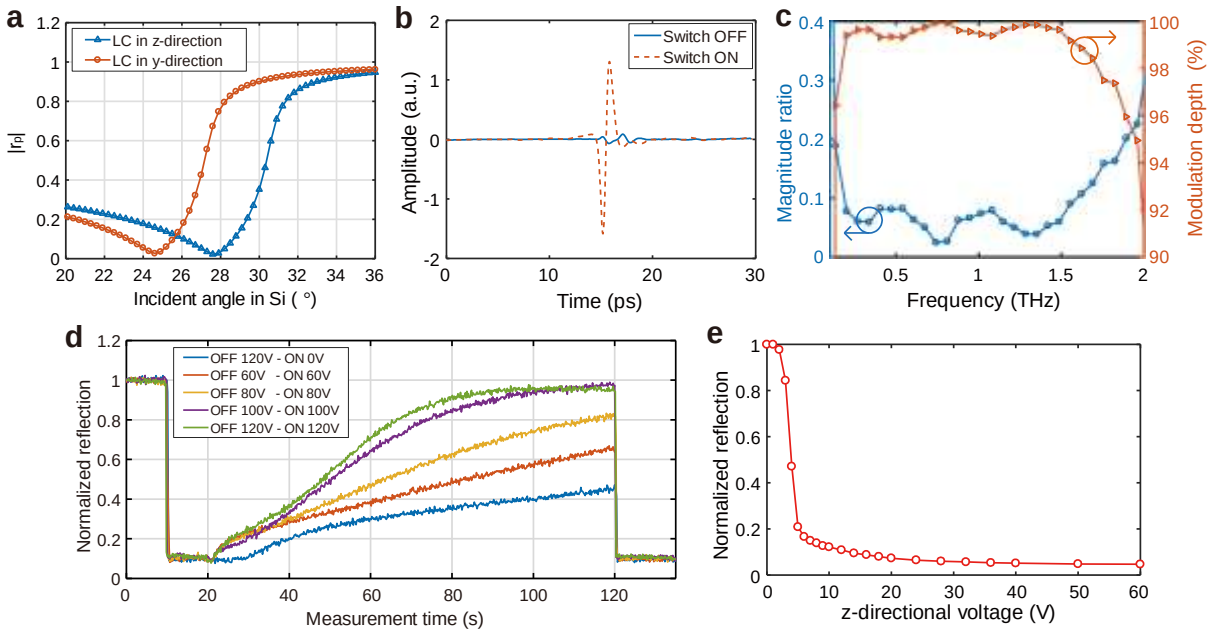

Figure 3. Theoretical calculation and experimental verification of the intensity modulation. **a**. Calculated reflection from the Si-LC interface as a function of incident angles to the Si-LC interface, when the LC molecules were aligned in the y- and z-directions respectively. **b**. Measured time-domain signals when the device was switch at OFF and ON states. **c**. The magnitude ratio between the OFF and ON states and the modulation depth in frequency-domain. **d**. Time response of the reflection under different OFF and ON voltages. **e**. Reflection under small z-directional voltages

We applied 120 V to the +U electrode and the p-reflections for the OFF and ON states were measured. The time-domain signals are shown in Figure 3b. The OFF state gave an almost zero reflection, indicating that the LC molecules had been fully rotated to the z-direction to reach the Brewster angle. Notice that when the upper Si-LC reflection meets the Brewster

condition, the lower LC-Si reflection also satisfies the Brewster condition to give a weak reflection, hence almost no multiple reflections were introduced. Switching the device ON dramatically increased in field strength, indicating the LC molecules were successfully rotated to the y-direction and the device was near the critical angle. The frequency-domain magnitude ratio is shown in Figure 3c, as well as the modulation depth calculated by $100\% \times (1 - I_{\mathrm{OFF}}/I_{\mathrm{ON}})$. The value is very close to the theoretical calculation and the result is basically achromatic. An average modulation depth of 99.6% was achieved for 0.2 -1.6 THz. The insertion loss was only due to the 3 dB transmission loss from entering and leaving the prism and the 2 dB loss from the near critical reflection. The reflection loss is mainly from the small absorption of the LC that attenuates the THz light. The lower frequency limit is mainly set by the LC thickness. The refracted beam in the LC layer becomes an evanescent wave when it undergoes total-internal reflection, with a penetration depth in the z-direction proportional to the wavelength. When the cell thickness is smaller than the penetration depth of a certain wavelength, reflection and transmission at the lower Si occur to reduce the modulation depth. Figure 3c shows that the 500 μm thickness of our device has almost no influence down to 0.2 THz. The high frequency limit was set by the signal-to-noise ratio. The OFF state attenuated the signal for over 20 dB (magnitude ratio <0.1) which has exceeded the dynamic range above 1.6 THz. As the reflection behavior is decided by the refractive index of the LC, according to the results in Figure 2, the actual upper bandwidth is expected to be over 3 THz (see Supporting Information Section 3).

To show how the device was actively switched in two directions, we measured the time response of the reflection under different ON and OFF voltages in Figure 3d. The LC was initially in the y-direction to give a high reflectivity which was normalized to 1. At 10 s the device was switched OFF to load the voltage in the z-direction. The signal immediately dropped. The 120V gave a response time less than the minimum time resolution of 170 ms in

this measurement, and all the other voltages fell within 510 ms. At 20 s the device was switched ON. The 0 V curve demonstrates the self-recovery process by the anchoring forces offered by SD1 alignment layers, which was very slow and the actual full recovery time was about 15 min. As mentioned in the introduction, this is common but also the biggest challenge of THz LC devices. In our device, the second y-directional voltage actively improved the recovery speed with increasing voltage. At 120 V, it took only 60s to reach 90% of the maximum amplitude, which is 15 times faster than the self-alignment. At 120 s, the device was switched OFF and all the curves dropped immediately. In the ON state, a higher voltage can theoretically further improve the speed. However, it was limited to 120V here due to the greater heat generation at higher voltages. Although the nematic-isotropic point of the RDP 94990 LC is as high as 85.9^0 C, the birefringence of the LC reduced with the increasing temperature below this point, which is a common characteristic of LCs[45]. Details about the temperature effect on the LC and the device performance are given in Supporting Information Section 4. The temperature effect on the reduced birefringence also explains the lower amplitude at the end of the ON state for the 120 V case in Figure 3d. Our test shows that the device performance was not affected up to 120 V. Higher voltages can be realized by optimizing the device from many aspects and will be given in the discussion section.

The device was not only working in a binary mode of ON and OFF states. Applying a lower z-directional voltage in the OFF state enables a gradual modulation. This is shown in Figure 3e. The reflection can be continuously tuned from 1 to 0.1 within 10 V. This is essential for applications requiring a robust and continuous control of different field strengths.

2.4. Linear-circular conversion

The quick change from the Brewster to critical angle also indicates great phase-modulation potential. The magnitude ratio and phase difference between the p- and s-reflections as a

function of incident angles were calculated in Figure 4a and 4b. An interesting point was found at the incident angle of 30^0 . When the LC was in the z-direction, the p-reflectivity was 36% of the s-component with a near zero phase difference. Rotating the LC into the y-direction increases the magnitude ratio to about 1 and the phase difference to 90^0 . This indicates the potential of actively switching between a linear and a circular output.

The setup was changed to a 30^0 incident angle, and linear light polarized at 45^0 to the p-direction (thus equal p- and s- projections) was illuminated the device. The magnitude ratio and phase difference between the reflected p- and s-components at ON and OFF states were measured and shown in Figure 4c and 4d. The values show a high degree match to the theoretical prediction. Both the magnitude ratio and phase difference under the two states were found to be basically achromatic from 0.4 THz to 1.8 THz. In the ON state, the phase difference was very close to 90^0 and the maximum dispersion was only $+6^0$ and -2^0 . The magnitude ratio was also very close to 1 with a variation less than 7%. The OFF state closely kept the magnitude ratio at around 0.37 and the phase below 11^0 away from 0^0 . The bandwidth limitation can still be explained by the above analysis. The frequencies below 0.4 THz were affected by the interference from the lower LC-Si reflection. The upper bandwidth was limited by the signal-to-noise ratio. The birefringence of the LC theoretically supports the conversion at least up to 3 THz.

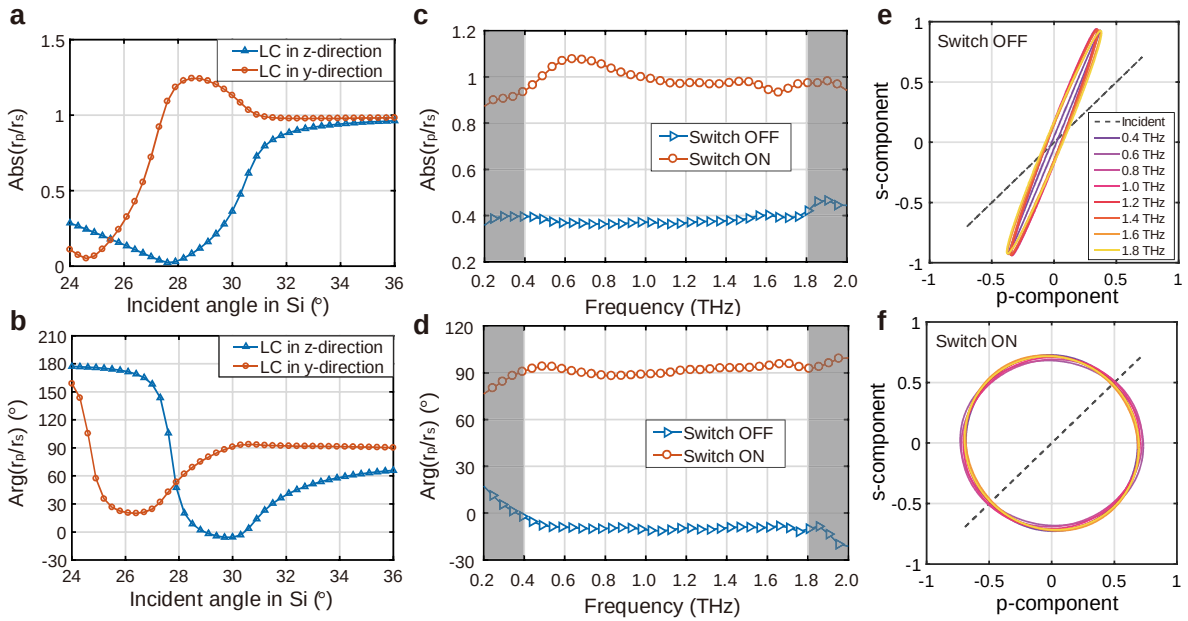

Figure 4. Amplitude and phase modulation by the proposed device. **a**. Theoretical magnitude ratio and **b**. phase difference between the reflected p- and s-reflection coefficients as a function of incident angles to the Si-LC interface, when the LC molecules were aligned in the y- and z-directions respectively. **c**. The measured magnitude ratio and **d**. phase difference between the p- and s-components in the frequency-domain when the device was at the OFF and ON states. The white regions show the bandwidth with a very small dispersion **e**. Polarization output from 0.4 THz to 1.8 THz at the OFF and **f**.ON state.

A more straightforward comparison for the polarization switch can be seen from Figure 4e and 4f. The reflections from 0.4 THz to 1.8 THz at OFF and ON states were plotted. An almost ideal linear state pointing at 20^0 to the s-direction was obtained at the OFF state, with a small ellipticity coming from the slight phase shift. The average *DoLP* (degree of linear polarization)[46] is 0.994. The ON state changed the device to a quarter-wave converter to output almost perfectly circular polarizations in the ultra-broad bandwidth, with the average *DoCP* (Degree of circular polarization) as high as 0.998. (The calculation of *DoLP* and *DoCP* is given in Supporting Information Section 5) The circular state was left-handed with the $+45^0$ polarized input, and can be easily changed to right-handed by rotating the incident THz beam to be -45^0 , perfectly satisfying the requirements in chiral spectroscopy. Moreover, as shown in Figure 4a and 4b, arbitrary elliptical polarizations can also be efficiently achieved by carefully selecting the incident angle and the incident polarization direction.

3. Conclusion

We have demonstrated the great modulation capability of the proposed LC device provided by the sensitive Brewster-critical angle change using both theoretical calculations and experimental verification. Both amplitude and phase can be highly efficiently modulated in an ultrabroad band manner, with the upper frequency limit set by the system and can be further extended to 3 THz theoretically. The introduced silicon-electrode design enables a two-directional electrical switch in the two fully perpendicular directions without any light absorption.

The achievement in the modulation efficiency and operational bandwidth is the key breakthrough of this work. For amplitude control, the modulation depth of 99.6% is not much different from the perfect state of 100%, and the insertion loss of 5 dB is also competitive with the state of the art[47–49]. The continuous and stable modulation at low voltages is more efficient than the optical or thermal based modulators[18,50]. For the polarization control, the broadband quarter-wave conversion has seldom been reported. Narrow-band quarter-wave conversion is already challenging in the THz range, as LC phase shifters need a sufficient cell depth[34] and metamaterials have a limited accuracy[22]. Using Fabry-Perot effect[24,27] or anisotropic reflection[51] extends the bandwidth to no more than 0.7 THz, which is still less than a half of this work. More importantly, in terms of controlling efficiency such as *DoLP* and *DoCP* in their reported range, we show a significantly better accuracy. The efficient and broadband manipulation on the amplitude and polarization make our device highly adaptive to a wide range of THz applications.

The bi-directional active electrical control is another important breakthrough compared to the state-of-art THz LC devices. The Si not only provides a large index contrast but also enables an E-field loading in both y- and z-directions. It behaved as a conductor in the ON state to transfer the z-directional E-field, and performed as a resistor in the OFF state to accelerate the

recovery process. Both states do not require any previously proposed electrodes such as ITO, graphene or metallic gratings to reduce the THz transparency. The upper voltage limit in the ON state was set by the heat generation that reduces the birefringence. A few optimizations on the structure can be made to increase the limit. For example, the use of a higher resistivity Si of 20 kΩ·cm can reduce the power consumption by a factor of 7. Reducing the electrode length in the x-direction to 1 cm further reduces the power by a factor of 5. Thinner Si wafers also directly increase the bulk resistivity (2 mm in this work). Furthermore, the resistance can also be increased by shortening the distance between the two electrodes in the y-direction, as long as the gap between the electrodes is larger than the beam spot. This also allows a lower bias voltage to produce an E-field of the same strength. All the aforementioned optimizations do not sacrifice any device performance metrics and would enable a field strength several times higher than reported in this work, hence a recovery time within few seconds can be reasonably expected. Moreover, the LC used in this work has a general birefringence of 0.17. Larger birefringence LCs broaden the distance between the two curves in Figure 3a and 4a, which can further enhance the amplitude and phase modulation ability and make the device more robust to the operation temperature. A comparison of the device performance by using larger birefringent LCs is discussed in Supporting Information Section 6.

4. Experimental Section

Device Fabrication: The two Si wafers were cleaned and etched by hydrogen fluoride followed by a standard photolithography process to make the aluminum electrodes of 200 nm thick. After that, they were annealed under 425^0 C in a N_2 flow for 10 min to improve the contact quality. SD1 (tetrasodium-5, 5 - ((1E, 1'E) - (2,2' - disulfonato - [1,1'-biphenyl] - 4,4' - diyl) bis (diazene - 2, 1 - diyl)) bis (2-hydroxybenzoate)) layers were spin coated on both wafers and exposed under a polarized UV light to initialize the alignment orientation in the y-direction. A self-built infrared microscope equipped with a MicronViewer 7290A camera was

used to align the two Si wafers to control the misalignment of the electrodes in the y-direction to be less than 20 μm. A 500 μm PVC spacer was sandwiched in-between the Si wafers and assembled. The RDP 94990 LC was filled in through an open slip. Finally, the slip was filled by another piece of PVC film and the device was sealed by epoxy.

Measurement: The transmission measurement to characterise the RDP 94990 LC. was performed by a self-built free-space THz-TDS system. The Si-LC-Si structure was placed in the focus of the THz beam and the transmitted signal was measured. The reference signal was taken by measuring the transmitted signal through another two Si wafers of the same thickness which were separated by air. A time-domain window is applied to both sample and reference signals to extract only the first transmitted pulse without multiple reflections. The sample/reference ratio in the frequency-domain can be expressed by Fresnel equations and solved analytically[52]. The reflection measurement was performed based on the fiber-based ellipsometry system built on Menlo K15. Three polarizers were used to make a precise control and detection of the polarization. A calibration algorithm was applied to improve the accuracy on the magnitude and phase detection. Details about the system, measurement and the algorithm can be found in our recent work on THz ellipsometry[53]. The incident angle was set to 22^0 and 30^0 in space, resulting in a 27.7^0 and 30^0 incident angle to the Si-LC interface for the intensity modulation and linear-quarter wave conversion, respectively.

Supporting Information

Supporting Information is available from the Wiley Online Library or from the author.

Acknowledgements

We would like to acknowledge Dr. H. K. Tsang for providing the infrared microscope, Dr. K. Ning for providing the annealing system, Mr. X. Xu for helping measure the IV characteristics of the samples. This work was supported by by the Research Grants Council of Hong Kong (project numbers 14206717 and 14201415), The Hong Kong Innovation and Technology Fund (project number ITS/371/16) and the Royal Society Wolfson Merit Award (EPM).

Received: ((will be filled in by the editorial staff))
Revised: ((will be filled in by the editorial staff))
Published online: ((will be filled in by the editorial staff))

References

[1] P. Gaal, K. Reimann, M. Woerner, T. Elsaesser, R. Hey, K. H. Ploog, *Phys. Rev. Lett.* **2006**, *96*, 187402.
[2] H. Hwang, N. Brandt, H. Farhat, A. L. Hsu, J. Kong, K. A. Nelson, *J. Phys. Chem. B* **2013**, *117*, 15819.
[3] J. Bock, Y. Fukuyo, S. Kang, M. Lisa Phipps, L. B. Alexandrov, K. O. Rasmussen, A. R. Bishop, E. D. Rosen, J. S. Martinez, H. T. Chen, G. Rodriguez, B. S. Alexandrov, A. Usheva, *PLoS One* **2010**, *5*, e15806.
[4] R. I. Stantchev, B. Sun, S. M. Hornett, P. A. Hobson, G. M. Gibson, M. J. Padgett, E. Hendry, *Sci. Adv.* **2016**, *2*, e1600190.
[5] S. Zhang, Y. shik Park, J. Li, X. Lu, W. Zhang, X. Zhang, *Phys. Rev. Lett.* **2009**, *102*, 023901.
[6] S. Zhang, J. Zhou, Y. S. Park, J. Rho, R. Singh, S. Nam, A. K. Azad, H. T. Chen, X. Yin, A. J. Taylor, X. Zhang, *Nat. Commun.* **2012**, *3*, 942.
[7] E. Castro-Camus, *J. Infrared, Millimeter, Terahertz Waves* **2012**, *33*, 418.
[8] E. Castro-Camus, M. B. Johnston, *J. Opt. A Pure Appl. Opt.* **2009**, *11*, 105206.
[9] T. Nagatsuma, S. Horiguchi, Y. Minamikata, Y. Yoshimizu, S. Hisatake, S. Kuwano, N. Yoshimoto, J. Terada, H. Takahashi, *Opt. Express* **2013**, *21*, 23736.
[10] L. L. Zhang, W. M. Wang, T. Wu, R. Zhang, S. J. Zhang, C. L. Zhang, Y. Zhang, Z. M. Sheng, X. C. Zhang, *Phys. Rev. Lett.* **2017**, *119*, 1.
[11] N. Karpowicz, J. Dai, X. Lu, Y. Chen, M. Yamaguchi, H. Zhao, X. C. Zhang, L. Zhang, C. Zhang, M. Price-Gallagher, C. Fletcher, O. Mamer, A. Lesimple, K. Johnson, *Appl. Phys. Lett.* **2008**, *92*, 90.
[12] H.-T. Chen, H.-T. Chen, W. J. Padilla, W. J. Padilla, J. M. O. Zide, J. M. O. Zide, A. C. Gossard, A. C. Gossard, A. J. Taylor, A. J. Taylor, R. D. Averitt, R. D. Averitt, *Nature* **2006**, *444*, 597.
[13] Y. Zhang, S. Qiao, S. Liang, Z. Wu, Z. Yang, Z. Feng, H. Sun, Y. Zhou, L. Sun, Z. Chen, X. Zou, B. Zhang, J. Hu, S. Li, Q. Chen, L. Li, G. Xu, Y. Zhao, S. Liu, *Nano Lett.* **2015**, *15*, 3501.
[14] B. Sensale-Rodriguez, R. Yan, M. M. Kelly, T. Fang, K. Tahy, W. S. Hwang, D. Jena, L. Liu, H. G. Xing, *Nat. Commun.* **2012**, *3*, 780.
[15] Y. Sun, R. Degl'Innocenti, D. A. Ritchie, H. E. Beere, L. Xiao, M. Ruggiero, J. A. Zeitler, R. I. Stantchev, D. Chen, Z. Peng, E. MacPherson, X. Liu, *Photonics Res.* **2018**, *6*, 1151.
[16] Y. Fan, N. H. Shen, F. Zhang, Q. Zhao, Z. Wei, P. Zhang, J. Dong, Q. Fu, H. Li, C. M. Soukoulis, *ACS Photonics* **2018**, *5*, 1612.
[17] Y. Fan, N. H. Shen, F. Zhang, Q. Zhao, H. Wu, Q. Fu, Z. Wei, H. Li, C. M. Soukoulis, *Adv. Opt. Mater.* **2019**, *7*, 1.
[18] E. P. J. Parrott, C. Han, F. Yan, G. Humbert, A. Bessaudou, A. Crunteanu, E. Pickwell-MacPherson, *Nanotechnology* **2016**, *27*, 205206.
[19] J. H. Shin, K. Moon, E. S. Lee, I. M. Lee, K. Hyun Park, *Nanotechnology* **2015**, *26*, 315203.
[20] T. L. Cocker, L. V Titova, S. Fourmaux, D. Brassard, M. A. El Khakani, F. A. Hegmann, *Appl. Phys. Lett.* **2010**, *97*, 221905.
[21] Y. Fan, N. H. Shen, F. Zhang, Z. Wei, H. Li, Q. Zhao, Q. Fu, P. Zhang, T. Koschny, C.

M. Soukoulis, *Adv. Opt. Mater.* **2016**, *4*, 1824.
[22] L. Cong, Y. K. Srivastava, H. Zhang, X. Zhang, J. Han, R. Singh, *Light Sci. Appl.* **2018**, *7*, 1.
[23] Q. Wang, E. Plum, Q. Yang, X. Zhang, Q. Xu, Y. Xu, J. Han, W. Zhang, *Light Sci. Appl.* **2018**, *7*, 1.
[24] L. Cong, N. Xu, J. Gu, R. Singh, J. Han, W. Zhang, *Laser Photonics Rev.* **2014**, *8*, 626.
[25] R.-H. Fan, Y. Zhou, X.-P. Ren, R.-W. Peng, S.-C. Jiang, D.-H. Xu, X. Xiong, X.-R. Huang, M. Wang, *Adv. Mater.* **2015**, *27*, 1201.
[26] N. K. Grady, J. E. Heyes, D. R. Chowdhury, Y. Zeng, M. T. Reiten, A. K. Azad, A. J. Taylor, D. a R. Dalvit, H.-T. Chen, *Science (80-.).* **2013**, *340*, 1304.
[27] Y. Zhang, Y. Feng, B. Zhu, J. Zhao, T. Jiang, *Opt. Express* **2015**, *23*, 27230.
[28] C.-S. Yang, T.-T. Tang, P.-H. Chen, R.-P. Pan, P. Yu, C.-L. Pan, *Opt. Lett.* **2014**, *39*, 2511.
[29] H. Y. Wu, C. F. Hsieh, T. T. Tang, R. P. Pan, C. L. Pan, *IEEE Photonics Technol. Lett.* **2006**, *18*, 1488.
[30] C. Y. Chen, T. R. Tsai, C. L. Pan, R. P. Pan, *Appl. Phys. Lett.* **2003**, *83*, 4497.
[31] C. Chao-Yuan, C. F. Hsieh, L. Yea-Feng, R. P. Pan, C. L. Pan, *Opt. Express* **2004**, *12*, 2625.
[32] M. Reuter, N. Vieweg, B. M. Fischer, M. Mikulicz, M. Koch, K. Garbat, R. Dąbrowski, *APL Mater.* **2013**, *1*, 012107.
[33] L. Wang, X. Lin, X. Liang, J. Wu, W. Hu, Z. Zheng, B. Jin, Y. Qin, Y. Lu, *Opt. Mater. Express* **2012**, *2*, 1314.
[34] L. Wang, X. Lin, W. Hu, G. Shao, P. Chen, L. Liang, B. Jin, P. Wu, H. Qian, Y. Lu, X. Liang, Z. Zheng, Y. Lu, *Light Sci. Appl.* **2015**, *4*, e253.
[35] Z. Liu, C.-Y. Huang, H. Liu, X. Zhang, C. Lee, *Opt. Express* **2013**, *21*, 6519.
[36] B. Vasić, D. C. Zografopoulos, G. Isić, R. Beccherelli, R. Gajić, *Nanotechnology* **2017**, *28*, 12402.
[37] Y. Wu, X. Ruan, C.-H. Chen, Y. J. Shin, Y. Lee, J. Niu, J. Liu, Y. Chen, K.-L. Yang, X. Zhang, J. Ahn, H. Yang, *Opt. Express* **2013**, *21*, 21395.
[38] X. Lin, J. Wu, W. Hu, Z. Zheng, Z. Wu, G. Zhu, F. Xu, B. Jin, Y. Lu, *AIP Adv.* **2011**, *1*, 032133.
[39] B. S. Y. Ung, X. Liu, E. P. J. Parrott, A. K. Srivastava, H. Park, V. G. Chigrinov, E. Pickwell-Macpherson, *IEEE Trans. Terahertz Sci. Technol.* **2018**, *8*, 209.
[40] J. Dai, J. Zhang, W. Zhang, D. Grischkowsky, *J. Opt. Soc. Am. B* **2004**, *21*, 1379.
[41] J. Lekner, *J. Phys. Condens. Matter* **1991**, *3*, 6121.
[42] J. Lekner, *J. Opt. Soc. Am. A* **1993**, *10*, 2059.
[43] N. Vieweg, N. Born, I. Al-Naib, M. Koch, *J. Infrared, Millimeter, Terahertz Waves* **2012**, *33*, 327.
[44] H. Park, E. P. J. Parrott, F. Fan, M. Lim, H. Han, V. G. Chigrinov, E. Pickwell-MacPherson, *Opt. Express* **2012**, *20*, 11899.
[45] R. P. Pan, C. F. Hsieh, C. L. Pan, C. Y. Chen, *J. Appl. Phys.* **2008**, *103*, 093523.
[46] S. Trippe, *J. Korean Astron. Soc.* **2014**, *47*, 15.
[47] Z. Chen, X. Chen, L. Tao, K. Chen, M. Long, X. Liu, K. Yan, R. I. Stantchev, E. Pickwell-MacPherson, J.-B. Xu, *Nat. Commun.* **2018**, *9*, 4909.
[48] X. Liu, E. P. J. Parrott, B. S.-Y. Ung, E. Pickwell-MacPherson, *APL Photonics* **2016**, *1*, 076103.
[49] G. Liang, X. Hu, X. Yu, Y. Shen, L. H. Li, A. G. Davies, E. H. Linfield, H. K. Liang, Y. Zhang, S. F. Yu, Q. J. Wang, *ACS Photonics* **2015**, *2*, 1559.
[50] T. Wen, D. Zhang, Q. Wen, Y. Liao, C. Zhang, J. Li, W. Tian, Y. Li, H. Zhang, Y. Li, Q. Yang, Z. Zhong, *Adv. Opt. Mater.* **2016**, *4*, 1974.
[51] X. Liu, X. Chen, E. P. J. Parrott, C. Han, G. Humbert, A. Crunteanu, E. Pickwell-

MacPherson, *APL Photonics* **2018**, *3*, 051604.
[52] M. Naftaly, R. E. Miles, *Proc. IEEE* **2007**, *95*, 1685.
[53] X. Chen, E. P. J. Parrott, Z. Huang, H. Chan, E. Pickwell-MacPherson, *Photonics Res.* **2018**, *6*, 768.

List of Figures

Figure 1. Optical arrangement and device configuration. **a.** Device assembled on a liquid-cooling cooper heat sink and illuminated by the THz light. **b.** 3D cross-section view of the y-z and x-y planes. **c.** 2D cross section view of the y-z plane in the OFF and ON states.

Figure 2. Characterized refractive index and absorption coefficient of the RDP 94990 LC in ordinary and extraordinary directions.

Figure 3. Theoretical calculation and experimental verification of the intensity modulation. **a**. Calculated reflection from the Si-LC interface as a function of incident angles to the Si-LC interface, when the LC molecules were aligned in the y- and z-directions respectively. **b**. Measured time-domain signals when the device was switch at OFF and ON states. **c**. The magnitude ratio between the OFF and ON states and the modulation depth in frequency-domain. **d**. Time response of the reflection under different OFF and ON voltages. **e**. Reflection under small z-directional voltages

Figure 4. Amplitude and phase modulation by the proposed device. **a**. Theoretical magnitude ratio and **b**. phase difference between the reflected p- and s-reflection coefficients as a function of incident angles to the Si-LC interface, when the LC molecules were aligned in the y- and z-directions respectively. **c**. The measured magnitude ratio and **d**. phase difference between the p- and s-components in the frequency-domain when the device was at the OFF and ON states. The white regions show the bandwidth with a very small dispersion **e**. Polarization output from 0.4 THz to 1.8 THz at the OFF and **f**.ON state.

Dr. Xuequan Chen received the B.Eng. degree (Honors) from University of Electronic Science and Technology of China in 2014. After that, he joined Prof. Emma Pickwell-MacPherson's Terahertz group in the Chinese University of Hong Kong for his PhD research and completed his PhD degree in 2018. He is now a postdoctoral fellow and continues his research in fast and accurate terahertz spectroscopy and imaging, ellipsometry and advanced terahertz devices.

Emma Pickwell-MacPherson studied Natural Sciences for her undergraduate degree at Cambridge University followed by an MSci in Physics where she specialized in semiconductor physics. She completed her PhD in 2005 with the Semiconductor Physics Group at Cambridge University, sponsored by TeraView Ltd. Her PhD work focused on understanding contrast mechanisms in terahertz images of skin cancer. More recently her research has encompassed developing THz devices, instrumentation and algorithms to improve THz metrology, ultimately with a view to applying THz imaging to biomedical applications.

Table of Content

The Brewster-critical angle switch is achieved by utilizing a nematic liquid crystal to realize ultrabroad band terahertz amplitude modulation and active linear-circular polarization control. The novel silicon electrode design provides perfect transparency to the terahertz light and bi-directional active control, which increases the modulation speed by a factor of 15.

Keyword terahertz modulation, active switch, quarter wave, liquid crystal, circular polarization, broadband

*Xuequan Chen, Kaidi Li, Rui Zhang, Swadesh Kumar Gupta, Abhishek Kumar Srivastava and Emma Pickwell-MacPherson**

Title Highly efficient ultra-broadband terahertz modulation using bi-directional switching of liquid crystals